Antitumor activity and pharmacodynamic properties of PX-478, an inhibitor of hypoxia-inducible factor-1α

Sarah Welsh,[1] Ryan Williams,[1] Lynn Kirkpatrick,[2] Gillian Paine-Murrieta,[1] and Garth Powis[1]

[1] Arizona Cancer Center, University of Arizona, Tucson, AZ and [2] ProlX Pharmaceuticals, Tucson, AZ

Abstract

The hypoxia-inducible factor-1 (HIF-1) transcription factor is an important regulator of tumor response to hypoxia that include increased angiogenesis, glycolytic metabolism, and resistance to apoptosis. HIF-1 activity is regulated by the availability of the HIF-1α subunit, the levels of which increase under hypoxic conditions. PX-478 (*S*-2-amino-3-[4′-*N*,*N*,-bis(2-chloroethyl)amino]phenyl propionic acid *N*-oxide dihydrochloride) is an inhibitor of constitutive and hypoxia-induced HIF-1α levels and thus HIF-1 activity. We report that PX-478 given to mice suppresses HIF-1α levels in HT-29 human colon cancer xenografts and inhibits the expression of HIF-1 target genes including vascular endothelial growth factor and the glucose transporter-1. PX-478 shows antitumor activity against established (0.15–0.40 cm^3) human tumor xenografts with cures of SHP-77 small cell lung cancer and log cell kills up to 3.0 for other tumors including HT-29 colon, PC-3 prostate, DU-145 prostate, MCF-7 breast, Caki-1 renal, and Panc-1 pancreatic cancers. Large (0.83 cm^3) PC-3 prostate tumors showed 64% regression, which was greater than for smaller tumors. The antitumor response to PX-478 was positively correlated with tumor HIF-1α levels ($P < 0.02$) and was accompanied by massive apoptosis. The results show that PX-478 is an inhibitor of HIF-1α and HIF-1 transcription factor activity in human tumor xenografts and has marked antitumor activity against even large tumor xenografts, which correlates positively with HIF-1α levels. [Mol Cancer Ther. 2004;3(3):233–244]

Introduction

Solid tumors with areas of hypoxia are the most aggressive and difficult tumors to treat (1). In addition to areas of hypoxia surrounding necrotic areas, solid tumors and even micrometastases have areas of hypoxia at the growing edge where tumor growth outstrips new blood vessel formation (2, 3). Hypoxic cancer cells present a major challenge to successful treatment (4) because they survive the hostile hypoxic environment by changing to a glycolytic metabolism (5), become resistant to programmed cell death (apoptosis; Refs. 6, 7), and migrate to less hypoxic areas of the body (metastasis; Ref. 8). Hypoxic cancer cells also produce several factors, including vascular endothelial growth factor (VEGF; Ref. 9) and basic fibroblast growth factor-2 (10), which stimulate new blood vessel formation from existing vasculature (angiogenesis) leading to increased tumor oxygenation and growth (11).

The cellular response to hypoxia is mediated through the hypoxia-inducible factor-1 (HIF-1) transcription factor (12, 13). HIF-1 is heterodimer consisting of HIF-α and HIF-1β (also known as the aryl hydrocarbon receptor nuclear translocator) subunits (14). There are three HIF-1 isoforms: HIF-1α plays a general role in hypoxia signaling, while HIF-2α and HIF-3α show a more restricted pattern of expression (15). HIF-1α and HIF-1β belong to the basic-helix-loop-helix Per-aryl hydrocarbon receptor nuclear translocator-SIM family of transcription factors (11). HIF-1α and HIF-1β associate in the cytosol prior to transport to the nucleus (16) where they bind to hypoxic-regulated element DNA sequences in the 3′ and 5′ regions of hypoxia-regulated genes (17). HIF-1β is constitutively expressed and its levels are not changed by hypoxia (12). HIF-1α is constitutively expressed, but under aerobic conditions, it is rapidly degraded by the ubiquitin-26S proteasome pathway so that HIF-1α levels are almost nondetectable (18). Under conditions of hypoxia, HIF-1α degradation is inhibited and HIF-1α protein levels increase, resulting in an increase in HIF-1 transactivating activity. The transcription of a wide variety of genes is increased by HIF-1 (12, 13) including genes for glycolytic metabolism (19), genes that promote erythropoiesis (20), genes that protect against apoptosis (21, 22), and genes that promote angiogenesis (10, 17, 23, 24).

HIF-1α protein levels depend on a series of oxygen-related post-translational modifications. The von Hippel-Lindau tumor suppressor protein (pVHL) binds to HIF-1α and organizes the assembly of a complex that activates E3 ubiquitin ligase resulting in the ubiquitination of HIF-1α, thus marking it for degradation by the 26S proteasome (25–27). pVHL binds the oxygen degradation domain of HIF-1α through conserved proline residues (Pro^{402} and Pro^{564} in human HIF-1α) that are hydroxylated by cytosolic HIF-1α-directed prolyl-4-hydroxylases (28–30). Prolyl-4-hydroxylases require O_2, Fe^{2+}, and 2-oxoglutarate or ascorbate as cofactors (28). When O_2 is limiting under hypoxic conditions, HIF-1α proline hydroxylation is inhibited resulting in decreased binding of pVHL, decreased HIF-1α degradation, and increased HIF-1α protein levels (30, 31). pVHL also acts in concert with

Received 11/25/03; revised 12/29/03; accepted 1/9/2004.

Grant support: NIH grants CA90821, CA52995, and CA98920.

The costs of publication of this article were defrayed in part by the payment of page charges. This article must therefore be hereby marked advertisement in accordance with 18 U.S.C. Section 1734 solely to indicate this fact.

Requests for Reprints: Garth Powis, Arizona Cancer Center, University of Arizona, 1515 North Campbell Avenue, Tucson, AZ 85724-5024. Phone: (520) 626-6408; Fax: (520) 626-4848. E-mail: gpowis@azcc.arizona.edu

histone deacetylase and other proteins as a transcriptional corepressor of HIF-1α transactivation under normoxic conditions (32). HIF-1α can bind to another E3 ubiquitin protein ligase, MDM2, which also degrades the tumor suppresser p53, resulting in HIF-1α ubiquitination and degradation and p53 stabilization (33, 34).

HIF-1 is necessary for tumor growth. Xenografts derived from HIF-1β-deficient hepatoma cells (24, 35) or HIF-1α-deficient Chinese hamster ovary cells (7) are less tumorigenic than parental cell xenografts. HIF-1α −/− knockout mouse embryonic stem (MES) cells also show decreased tumor growth compared with wild-type MES cells (36, 37), although one study reported increased tumor growth and decreased hypoxia-induced apoptosis of HIF-1α −/− MES cells (38). Reintroduction of the intact VHL gene into cells lacking functional VHL derived from renal carcinomas restores HIF-1α to normoxic levels (39, 40) and decreases tumorigenicity (41).

HIF-1α is found at increased levels in a wide variety of human primary tumors compared with corresponding normal tissue (42–49). The importance of HIF-1α to human cancer is demonstrated by the high incidence of tumors such as renal cell carcinoma, pheochromocytoma, and hemangioblastoma of the central nervous system in individuals with loss of function of both alleles of the VHL gene leading to elevated HIF-1α levels (50). In addition, most cases of sporadic renal cell carcinoma are associated with an early loss of function of the VHL gene and increased HIF-1α levels (39, 51). While most work has focused on the role of HIF-1α in increasing tumor growth, HIF-2α is also up-regulated in human cancer (24), particularly in renal cancer (52). However, HIF-2α is a constitutively expressed protein that does not exhibit oxygen-dependent degradation and endogenous HIF-2α does not stimulate the transcription of typical HIF-1 target genes (53). Thus, it has been suggested that HIF-2α may have different functions to HIF-1α, unrelated to the hypoxia response (54).

PX-478 (*S*-2-amino-3-[4′-*N*,*N*,-bis(2-chloroethyl)amino]-phenyl propionic acid *N*-oxide dihydrochloride) is a novel agent that suppresses constitutive and hypoxia-induced levels of HIF-1α in cancer cells (55). We have investigated the antitumor activity of PX-478 against human tumor xenografts and its toxicity, pharmacokinetics, and pharmacodynamics in mice. We have found that PX-478 inhibits HIF-1α and HIF-1-regulated genes and has antitumor activity against several human tumor xenografts that is related to HIF-1α levels in the tumors.

Materials and Methods

Antitumor Studies

MCF-7 human breast cancer, HT-29 colon cancer, PC-3 prostate cancer, DU-145 prostate cancer, OvCar-3 ovarian cancer, A-549 non-small cell lung cancer, SHP-77 small cell lung cancer, and Caki-1 renal cancer cell lines were obtained from the American Tissue Type Collection (Rockville, MD). Panc-1, MiaPaCa, and BxPC-3 pancreatic cancer cell lines were kindly supplied by Dr. Dan Von Hoff (University of Arizona, Tucson, AZ). The cells were grown in humidified 95% air, 5% CO_2 at 37°C in DMEM supplemented with 10% fetal bovine serum. Cells (10^7) in log cell growth were injected s.c. in 0.2 ml Matrigel (BD Biosciences, Palo Alto, CA) into the flanks of *scid* mice. Female mice that were to receive the estrogen-dependent MCF-7 breast cancer cell line (56) were implanted s.c. in the back with a 90-day 17-β-estradiol release pellet (Innovative Research of America, Sarasota, FL) a day before the tumor cells. PX-478 was prepared fresh each day in 0.9% NaCl as a 10 or 20 mg/ml solution and given to the mice by various routes and schedules within 30 min of preparation. Tumor diameters at right angles (d_{short} and d_{long}) were measured twice weekly with electronic calipers and converted to volume by the formula: volume = $d_{short}^2 \times d_{long} \div 2$ (57). When the tumors reached between 150 and 830 mm^3, the mice were stratified into groups of eight animals having approximately equal mean tumor volumes and drug administration was begun. Tumor volume was measured twice weekly until the tumor reached 2000 mm^3 or more or became necrotic, when the animals were euthanized. Animals were weighed weekly. Tumor growth rate was calculated from the linear portion of the least squares regression of the cube root of the tumor volume. Tumor regression was calculated as the maximum decrease in tumor volume from the start of treatment and tumor growth delay was calculated as the time for the mean tumor volume to reach twice the non-drug-treated mean tumor volume at the start of PX-478 treatment. Log_{10} cell kill was calculated by the formula: log_{10} cell kill = tumor growth delay (days) ÷ tumor doubling time (days) × 3.32; Ref. 58). One-way analysis of variance using the general linear model (59) was used to test for the effect of treatment on tumor growth rate and growth delay. Correlations between tumor HIF-1α levels as continuous variables and antitumor activity measured by tumor regression, growth delay, and log_{10} cell kill were by linear regression.

Pharmacodynamic Studies

HT-29 colon cancer cells (10^7) were injected s.c. into the flanks of male *scid* mice and allowed to grow to ~300 mm^3. The animals received a single i.p. dose of PX-478 (100 mg/kg) in 0.9% NaCl and were killed at various times. Blood was collected into heparinized tubes for preparation of plasma, which was stored at −20°C, and tumors were excised and fixed in 5% buffered formaldehyde for immunohistochemistry.

Immunohistochemistry

Paraffin-embedded tissue sections were heated at 60°C for 30 min and rehydrated through xylene and graded alcohols. Antigen retrieval was performed as dictated by the individual proteins as follows: 40 min at pH 9.0 for HIF-1α, 90 min at pH 9.0 for HIF-2α, 20 min at pH 6.0 for VEGF and factor VIII-related antigen, 15 min at pH 6.0 for glucose transporter-1 (Glut-1), and 25 min at pH 9.0 for cleaved caspase-3. The slides were blocked for 30 min in 4% milk, 1% goat serum, and 0.1% thimerosal in PBS. After blocking, the slides were processed using a 3,3′-Diaminobenzidine Basic Detection Kit (Ventana

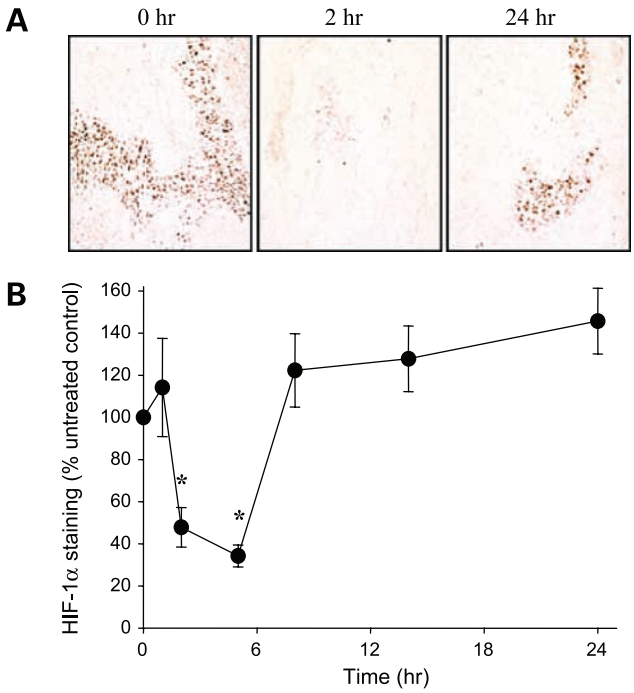

Figure 1. Inhibition of tumor HIF-1α by PX-478. Male *scid* mice were injected s.c. in the flank with 10^7 HT-29 colon cancer cells. The tumors were allowed to grow to ~300 mm^3 and the mice were treated with PX-478 at a single i.p. dose of 120 mg/kg. The animals were euthanized at various times and the tumors were excised and taken for HIF-1α staining by immunohistochemistry. **A,** typical sections showing HIF-1α staining in the untreated control (*0 hr*), HIF-1α staining (*2 hr*), and return to control HIF-1α staining (*24 hr*). **B,** staining was quantified by digital image analysis and expressed as percentage relative to nontreated tumor. *Points,* means of four animals; *bars,* SE. *, $P < 0.05$, compared with nontreated control.

Medical Systems, Tucson, AZ). Endogenous peroxidase activity was quenched using a hydrogen peroxide-based inhibitor included in the kit, and endogenous biotin was blocked using an Avidin/Biotin Blocking Kit (Ventana Medical Systems). Using an ES Automated Slide Stainer (Ventana Medical Systems), the slides were incubated for 32 min at 42°C with the following primary antibodies: mouse monoclonal anti-human HIF-1α (Transduction Labs, Lexington, KY) at 10 μg/ml, rabbit polyclonal anti-human HIF-2α (Novus Biologicals, Littleton, CO) at 3 μg/ml, rabbit polyclonal anti-human VEGF (Santa Cruz Biotechnology, Santa Cruz, CA) at 5 μg/ml, rabbit polyclonal anti-human factor VIII-related antigen (Dakopatts, Santa Barbara, CA) at 1:800 dilution, rabbit polyclonal anti-human cleaved caspase-3 (Cell Signaling Technology, Beverly, MA) at 1 μg/ml, and rabbit polyclonal anti-human Glut-1 (Chemicon International, Inc., Temecula, CA) at 1:2700 dilution. A biotinylated universal secondary antibody, which recognized mouse IgG/IgM or rabbit IgG, was then applied followed by horseradish peroxidase-conjugated avidin, 3,3′-diaminobenzidine/hydrogen peroxide, and a copper enhancer. The slides were dehydrated through graded alcohols, toluene, and xylene and coverslipped using Vectamount (Vector Laboratories, Inc., Burlingame, CA). Six 24-bit three-color images of each tumor section were captured in RGB TIFF format using a Nikon TE300 inverted microscope (Nikon, Melville, NY) with 10× Plan Apo objective lens (AG Heinze, Chandler, AZ) using a Roper Scientific Coolsnap digital camera (Princeton Instruments, Trenton, NJ). Images were quantitated using the Simple PCI digital image analysis software package (Compix Imaging Systems, Pittsburgh, PA). The low threshold for analysis was set using a tissue section stained with a nonreactive antibody and the staining was normalized to the staining of an on-slide control of hypoxic MCF-7 breast cancer cells. Microvessel density was measured by light microscopy of factor VIII-related antigen-stained sections using the criteria of Weidner *et al.* (60).

Western Blotting

Cell nuclear extracts were prepared using NE-PER Nuclear and Cytoplasmic Extraction Reagents (Pierce Chemical Co., Rockford, IL). Western blotting was performed as described previously (61) using 1 μg/ml mouse anti-human HIF-1α antibody (Transduction Labs). Anti-mouse horseradish peroxidase-conjugated secondary antibody (Amersham Pharmacia, Uppsala, Sweden) was used at a dilution of 1:5000 for detection by chemiluminescence.

Serum VEGF and Erythropoietin Measurement

The amount of VEGF in serum was determined using human and mouse VEGF ELISA kits that measure $VEGF_{165}$ and $VEGF_{121}$ isoforms (R&D Systems, Inc., Minneapolis, MN). The amount of erythropoietin in mouse serum was measured using a kit for human erythropoietin (Human EPO-ELISA; R&D Systems) that cross-reacts with mouse erythropoietin, and mouse erythropoietin was used as a standard.

Pharmacokinetic Studies

Male C57BL/6 mice were given PX-478 at a dose of 150 mg/kg as a freshly prepared 15 mg/ml solution in 0.9% NaCl either i.v., i.p., or by p.o. gavage. The mice were killed at various times, and blood was collected into heparinized tubes and plasma was prepared. Plasma (0.2 ml) was immediately mixed with an equal volume of 0.1% trifluoroacetic acid (TFA) in acetonitrile and centrifuged at 15,000 × *g* for 5 min at 4°C. Supernatant solution (50 μl) was injected into the high-pressure liquid chromatograph (HPLC) for the PX-478 assay. The HPLC system comprised a Brownlee Cyano Spheri-5 250 mm column eluted at a flow of 1.5 ml/min with TFA/acetonitrile/H_2O (0.1:10:99) for 20 min followed by a 15 min gradient to 100% of 0.1% TFA in acetonitrile. Fluorescence detection was employed at an excitation wavelength of 200 nm and emission wavelength of 365 nm. PX-478 was eluted at 4.6 min with a lower limit for detection of 10 μg/ml plasma. To measure plasma protein binding, PX-478 was added at 500 μg/ml to fresh mouse plasma at 4°C and an ultrafiltrate was prepared using a 10,000 molecular weight cutoff centrifugal filter (Centricon 10; Millipore, Billerica, MA).

Results

Inhibition of HIF-1α in Tumors

Staining for HIF-1α by immunohistochemistry showed that HIF-1α was unevenly distributed throughout tumors and was predominantly nuclear with little cytoplasmic HIF-1α staining (Fig. 1A). Large tumors showed more areas of HIF-1α staining than small tumors, which was associated with increased areas of necrosis in the large tumors. For this reason, HIF-1α staining was routinely measured in tumor xenografts between 150 and 300 mm^3 before areas of necrosis became a prominent feature. Significant HIF-2α staining was not observed in any of the tumors. Where HIF-2α was detected, it was present in macrophage-like cells in areas of inflammation and some were distributed throughout the tumor. PX-478 was given as a single i.p. dose of 120 mg/kg to *scid* mice bearing s.c. HT-29 human colon tumor xenografts. The mice were killed at various times and the tumors were removed, fixed, and stained for HIF-1α. HIF-1α staining was quantified by digital image analysis and expressed relative to the staining of non-drug-treated tumor xenografts (Fig. 1B). Administration of PX-478 to mice resulted in a significant decrease in tumor HIF-1α staining, with a maximum decrease (± SE) at 5 h to 29.3 ± 10.4% of non-drug-treated tumor values ($P < 0.05$). HIF-1α levels had returned to non-drug-treated values by 8 h after administration of PX-478 ($P > 0.05$). The HIF-2α staining in tumor macrophages was not affected by PX-478.

Table 1. Posttreatment effects of PX-478 treatment on HT-29 HIF-1α and its downstream target proteins

Protein control	Staining (%)	PX-478-treated staining (%)	*P*
HIF-1α	100.0 ± 6.0	80.2 ± 24.2	0.404
Caspase-3	100.0 ± 4.4	696.8 ± 57.5	0.009
Glut-1	100.0 ± 1.3	85.6 ± 4.4	0.012
VEGF	100.0 ± 2.4	104.0 ± 6.8	0.571

Note: *scid* mice with 300 mm^3 HT-29 tumor xenografts were given PX-478 i.p. at 100 mg/kg/day for 5 days and tumors were removed 3 days later for immunohistochemical staining of HIF-1α and its target proteins. Staining was quantitated by digital image analysis and expressed relative to control values as 100%. Values are means ± SE of four mice in each group.

Inhibition of HIF-1 Target Genes

Immunohistochemical staining for Glut-1, the expression of which is regulated by HIF-1 (62), showed decreased Glut-1 in tumors from mice treated with PX-478 at a single i.p. dose of 120 mg/kg. The decrease was delayed and sustained compared with the decrease in HIF-1α, with a maximum decrease (± SE) at 14 h to 23.7 ± 4.5% of non-drug-treated tumor values and was still at 56.0 ± 5.9% at 48 h ($P < 0.05$; Fig. 2A). Staining for tumor VEGF, the expression of which is also regulated by HIF-1 (63), showed a decrease (± SE) at 2 h to 61.7 ± 16.9% of non-drug-treated tumor values ($P < 0.05$) with recovery to above non-drug-treated values by 5 h (Fig. 2B). There was no change in staining for cleaved caspase-3, a measure of apoptosis (64), or in microvessel density, a measure of angiogenesis (60), up to 24 h after treatment with PX-478. Three days after a course of PX-478 at 100 mg/kg/day i.p. for 5 days as used for the antitumor studies, there was no significant change

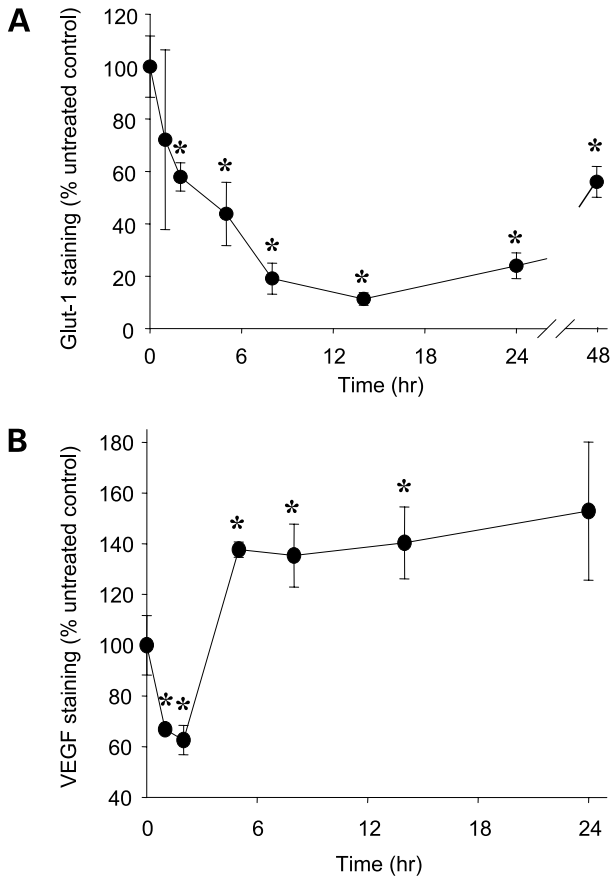

Figure 2. Inhibition of HIF-1 target gene expression by PX-478. Male *scid* mice with s.c. HT-29 human colon tumor xenografts were treated with PX-478 at a single i.p. dose of 120 mg/kg. Tumors were excised and stained by immunohistochemistry for Glut-1 (**A**) and VEGF (**B**). Staining was quantified by digital image analysis and expressed as percentage relative to nontreated tumor. *Points,* means of four animals; *bars,* SE. *, $P < 0.05$, compared with untreated control.

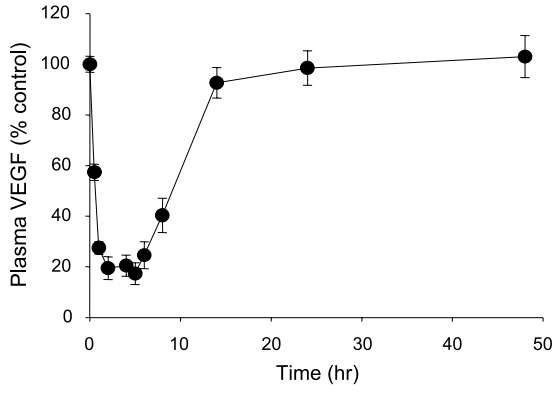

Figure 3. PX-478 lowers plasma VEGF levels in the mouse. Male *scid* mice were treated with PX-478 at a single i.p. dose of 120 mg/kg and plasma VEGF levels were measured at various times. *Points,* means of three mice at each time point expressed as percentage relative to non-treated tumor; *bars,* SE.

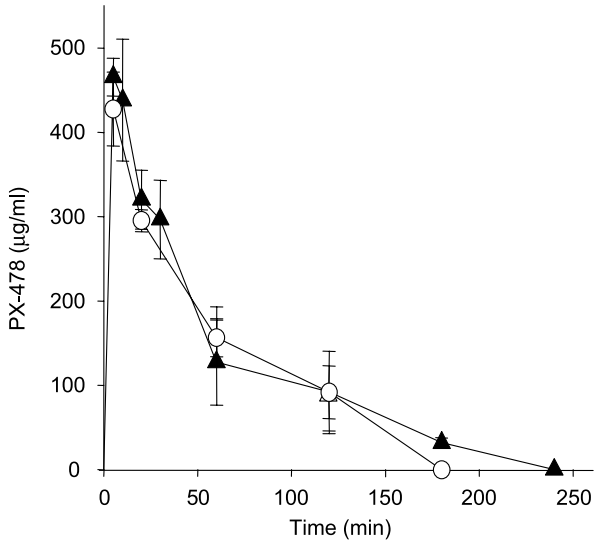

Figure 4. Pharmacokinetics of PX-478 in the mouse. Nontumor male C57BL/6 mice were given PX-478 (120 mg/kg) by the i.p. (○) or i.v. (▲) routes. Plasma PX-478 was measured by HPLC. *Points,* means of three mice; *bars,* SE.

in tumor HIF-1α or VEGF staining and a small (14.4%) but significant ($P < 0.05$) decrease in tumor Glut-1 staining (Table 1). At the same time, there was a 7.2 ± 0.8-fold increase, compared with untreated tumors, in staining for cleaved caspase-3 and an increase in HIF-2α-stained tumor macrophages, indicating that the tumor was undergoing massive apoptosis.

Mouse plasma was assayed for human and mouse VEGF and mouse erythropoietin by specific ELISA. No human VEGF from the HT-29 human tumor xenografts could be detected in the mouse plasma. On treatment with a single i.p. dose of PX-478 of 120 mg/kg, there was a rapid decrease (± SE) in mouse plasma VEGF to 18.8 ± 2.2% of control values at 2 h ($P < 0.01$; Fig. 3). There was no detectable change in mouse plasma erythropoietin, another HIF-1α-regulated protein that stimulates hemoglobin production (20), up to 24 h after the administration of PX-478 (data not shown).

PX-478 Pharmacokinetics

The half-life of PX-478 in sodium phosphate buffer (50 mM) was 25 h at pH 2.0 and 2.1 h at pH 6.5. PX-478 is a dihydrochloride salt, and when dissolved in unbuffered 0.9% NaCl or water, it gave an acid solution and the half-life was 8.8 h. The half-life of PX-478 was 37 min in fresh mouse plasma and 420 min in the supernatant from mouse plasma treated at 98°C for 15 min to denature proteins. These values probably reflect the alkaline nature of mouse plasma, which becomes acid on heat treatment. Studies of the binding of PX-478 to mouse plasma proteins gave a recovery of PX-478 in the ultrafiltrate corrected for degradation during the 2 h centrifugation of 102.8 ± 7.1%. Thus, PX-478 is not bound to mouse plasma. Pharmacokinetic studies were conducted in male C57BL/6 mice given PX-478 i.v., i.p., or by p.o. gavage at a single dose of 150 mg/kg (Fig. 4). The peak plasma concentration of PX-478 following i.p. administration was 428 μg/ml, which occurred within 5 min of administration, and the half-life was 47 min. The pharmacokinetic parameters of i.p. PX-478 were similar to PX-478 given i.v. and the bioavailability was 91% (Table 2). PX-478 given p.o. had a bioavailability of 86%.

Antitumor Activity

The antitumor activity of PX-478 was investigated using s.c. implanted human tumor xenografts in *scid* mice. The approximate maximum tolerated dose of PX-478 given to *scid* mice was 250 mg/kg as a single i.p. dose and 140 mg/kg/day as five daily i.p. doses. Treatment of mice with established 120 mm^3 OvCar-3 ovarian cancer tumor xenografts with PX-478 with 100 mg/kg/day i.p. for 5 days gave a 99% tumor regression and a tumor growth delay of 57 days (Fig. 5A). Treatment of mice with SHP-77 human small cell lung cancer xenografts with PX-478 on the same schedule was curative with no histologically detectable tumor cells at the site of implantation at 100 days after the termination of treatment (Fig. 5B). Another sensitive tumor was MCF-7 breast cancer, where PX-478 at 100 mg/kg/day i.p. for 5 days to mice with 180 mm^3 tumors gave a 48% tumor regression and a tumor growth delay of 43 days (Fig. 5B). PC-3 prostate cancer is a rapidly growing tumor that was responsive to PX-478. For PX-478 at a dose of 100 mg/kg/day i.p. for 5 days to mice with 138 mm^3 tumors, there was a 71% regression and a tumor growth delay of 30 days. In another study with the same PX-478 treatment, very large PC-3 tumors of 830 mm^3 showed a 64% tumor regression treatment, which was larger than with 320 mm^3 tumors (Fig. 5C). Table 3 summarizes the antitumor activity of PX-478 given by a daily i.p. schedule for 5 days against a variety of established human tumor xenografts and shows that $\log_{10}$ cell kills of up to 3.0 can be obtained by this schedule. It is noteworthy that tumor regressions were delayed until 3–10 days after treatment with PX-478 was complete. A-549

Table 2. Pharmacokinetic parameters of PX-478 in mice

Route	Compound	C_{max} (μg/ml)	$T_{1/2}$ (min)	AUC (μg/ml)	Cl (ml/min/kg)	Vss (ml/kg)	F
i.v.	PX-478	428	60.6	31918	4.7	380	–
i.p.	PX-478	465	47.4	29122	–	–	0.91
p.o.	PX-478	158	27.9	27474	–	–	0.86

Note: Mice were administered 150 mg/kg PX-478 via different routes listed. The pharmacokinetic parameters are as follows: C_{max}, maximum plasma concentration; $T_{1/2}$, half life; AUC, area under the curve from time 0 min to infinity; Cl, plasma clearance; Vss, steady state volume of distribution; F, bioavailability as compared to i.v. administration.

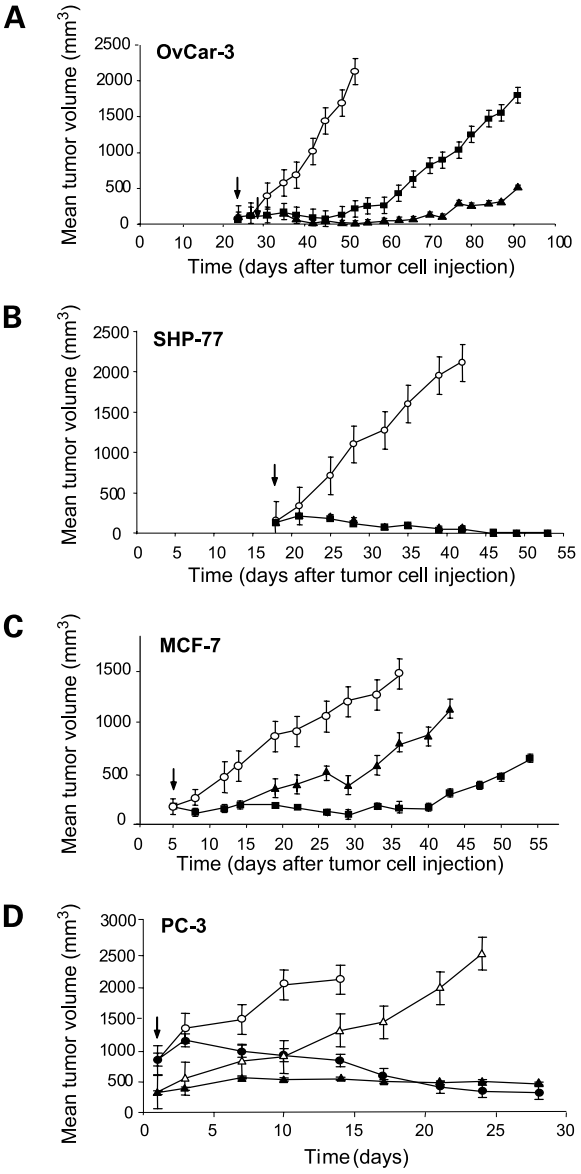

Figure 5. Antitumor activity of PX-478. **A,** female *scid* mice were implanted s.c. in the flank with 10^7 OvCar-3 human ovarian cancer cells. When the tumors reached 120 mm^3 at day 24 (as shown by the *arrow*), the mice received either vehicle (○) or PX-478 i.p. at 100 mg/kg/day (▲) or 80 mg/kg/day (■) for 5 days. Tumor diameter in two directions (d_{short} and d_{long}) was measured twice weekly with calipers and tumor volume was calculated. **B,** female *scid* mice were implanted s.c. in the flank with 10^7 SHP-77 human small cell lung cancer cells. When the tumors reached 160 mm^3 at day 18 (as shown by the *arrow*), the mice received either vehicle (○) or PX-478 i.p. at 100 mg/kg/day (▲) or 75 mg/kg/day (■) for 5 days. There was no evidence of tumor when the drug-treated animals were examined histologically for evidence of tumor at the implantation site on day 100 after drug treatment. **C,** female *scid* mice received a s.c. implant of a 90-day 17-β-estradiol release pellet 1 day before s.c. implantation in the flank of 10^7 MCF-7 human breast cancer cells. When the tumors reached 180 mm^3 at day 5 (as shown by the *arrow*), the mice received either vehicle alone (○) or PX-478 i.p. as a single dose of 200 mg/kg (▲) or as five daily doses of 80 mg/kg (■). **D,** male *scid* mice were implanted s.c. in the flank with 10^7 PC-3 prostate cancer cells. When the tumors reached 320 mm^3 (○ and ●) or 830 mm^3 (△ and ▲; in both cases denoted as day 1 by the *arrow*), dosing was begun with vehicle (○ and △) or PX-478 i.p. at 100 mg/kg/day (● and ▲) for 5 days. *Points,* mean calculated tumor volumes of eight mice in each group; *bars,* SE.

human non-small cell lung cancer showed no antitumor response to PX-478. Table 4 shows the antitumor activity of some clinically used anticancer drugs against tumor xenografts of the sizes used for PX-478. None of the drugs tested showed antitumor activity approaching that of PX-478.

Schedule Dependency

Several different schedules of PX-478 administration were examined (Table 5). A single i.p. administration of PX-478 of 120 mg/kg to mice with MCF-7 breast cancer xenografts gave a $\log_{10}$ tumor cell kill of 0.9; when given i.p. at 80 mg/kg/day for 5 doses, the $\log_{10}$ tumor cell kill was 2.3; and when given at 80 and 120 mg/kg every other day for five doses, $\log_{10}$ tumor cell kills were 2.0 and 2.5, respectively. Continuous weekly i.p. administration of PX-478 at 120 mg/kg or twice weekly administration at 60 mg/kg gave cumulative $\log_{10}$ tumor cell kills of 3.4 and 2.5, respectively.

Antitumor Activity and Tumor HIF-1α Levels

HIF-1α staining in tumor xenografts paralleled that in hypoxic cancer cell lines from which they were derived with xenografts from cell lines with high levels of HIF-1α showing the highest HIF-1α staining (Fig. 6A). Linear regression analysis of tumor xenograft HIF-1α staining measured as low, medium, or high gave significant positive correlations, with PX-478 antitumor activity measured as tumor regression ($P = 0.016$), tumor growth delay ($P = 0.014$), or $\log_{10}$ cell kill ($P = 0.007$; Fig. 6, B and C).

Toxicity of PX-478

The major acute toxicity of PX-478 given daily for 5 days to nonimmunodeficient C57BL/6 mice was neutropenia (Table 6). There was no decrease in the number of platelet or RBC and no change in serum liver enzymes or blood urea nitrogen or creatinine, indicating the absence of acute liver or renal toxicity. There was acute weight loss accompanied with a decrease in food intake (data not shown), but the mice appeared otherwise healthy and remained active. The weight loss had recovered by 19 days and neutropenia by 35 days after the end of dosing (Fig. 7). There was a delayed transient decrease in hemoglobin and in the number of RBC at 14 days after dosing, but this had recovered by 25 days. Continuous weekly or twice weekly dosing of PX-478 gave lymphocytopenia, moderate neutropenia, and no weight loss until 5 weeks (data not shown). There was a transient decrease in hemoglobin and RBC at 1–2 weeks and this recovered even with continuous dosing. The decrease in hemoglobin was not caused by a decrease in erythropoietin by PX-478, because plasma levels of erythropoietin increased at this time presumably in response to the decreases in hemoglobin levels (Fig. 8). Plasma VEGF levels were not changed at these later times after PX-478 dosing (data not shown).

Discussion

We have reported previously that PX-478 suppresses hypoxia induction of HIF-1α in cancer cell lines and suppresses constitutive HIF-1α in cells that have lost pVHL (55). The present study extends the work on PX-478 in

Table 3. Antitumor activity of PX-478 against human tumor xenografts in *scid* mice

Tumor	Initial tumor volume (mm^3)	PX-478 (mg/kg/day)	Schedule	Regression (%)	Growth delay (days)	Log_{10} cell kill	*P*
OvCar-3 ovarian	120	100	Q1D × 5	99	57	3.0	*
		80	Q1D × 5	42	31	1.6	*
HT-29 colon	410	120	Q1D × 5	0	21	2.0	*
		80	Q1D × 5	0	16	1.6	*
		60	Q1D × 9	19	22	2.4	
PC-3 prostate	138	100	Q1D × 5	71	30	2.0	*
		60	Q1D × 5	2	10	0.7	*
DU-145 prostate	310	100	Q1D × 5	50	24	2.4	*
		60	Q1D × 5	40	15	1.5	*
MCF-7 breast[a]	180	100	Q1D × 5	48	43	1.0	*
		80	Q1D × 5	33	27	1.2	*
Caki-1 renal	250	100	Q1D × 5	44	54	1.8	*
		60	Q1D × 5	6	12	0.4	*
Panc-1 pancreatic	125	100	Q1D × 5	40	35	2.0	*
		60	Q1D × 5	10	27	0.9	*
MiaPaCa pancreatic	288	100	Q1D × 5	20	6	0.2	*
		60	Q1D × 5	4	3	0.1	*
BxPC-3 pancreatic	100	100	(Q1D × 5) × 2[b]	20	30	0.8	*
		75	(Q1D × 5) × 2[b]	20	17	0.5	*
A-549 non-small cell lung	370	100	Q1D × 5	0	2	0.1	
		60	Q1D × 5	0	0	0	
SHP-77 small cell lung	160	100	Q1D × 5	100	>100	Cure	*
		75	Q1D × 5	100	>100	Cure	*

Note: Mice were implanted s.c. with 10^7 tumor cells. When the tumor volume reached 100 to 300 mm^3, the mice were randomized into groups of eight and i.p. drug treatment started at the doses shown.
[a]Female mice implanted with 17-β-estradiol 60-day slow release pellets.
[b]Course repeated at 45 days.
*$P < 0.05$, compared with non-drug-treated control tumor growth rate.

cancer cell lines into mice with tumor xenografts. PX-478 given at doses that caused tumor growth delay suppressed HIF-1α levels up to 71% in HT-29 human tumor xenografts. The decrease in HIF-1α was associated with a decreased expression of the HIF-1 downstream target genes. The expression of VEGF, an important angiogenic factor produced by solid tumors leading to the development of new blood vessels from preexisting capillary beds (65) and an autocrine factor for hematological tumors (66), was decreased by PX-478 by 38% ($P < 0.05$). The expression of Glut-1, a ubiquitously expressed member of a family of transport proteins responsible for the facilitated diffusion of hexoses into mammalian cells (67, 68), was decreased by 76% ($P < 0.05$). Glut-1 inhibition was maintained for at least 48 h. While many *glut* genes are activated post-translationally by acute hypoxia (67), only *glut-1* shows a HIF-1-dependent increase in transcription in response to prolonged hypoxia (67). Increased Glut-1 expression has been associated with aggressive tumor growth and decreased metastasis free survival of patients with cervical cancer (69). Interestingly, the expression of HIF-2α in tumor macrophages was not inhibited by PX-478. Unlike HIF-1α,

Table 4. Antitumor activity of other drugs against human tumor xenografts in *scid* mice

Drug (i.p. dose)	Schedule	Tumor	Initial tumor volume (mm^3)	Regression (%)	Growth delay (days)	Log_{10} cell kill	*P*
Taxol (21 mg/kg)	Q2D × 5	A-549 non-small cell lung	370	0	21	0.9	*
Mitoxantrone (0.34 mg/kg)	Q1D × 5	DU-145 prostate	600	0	6	0.6	*
Gemcitabine (180 mg/kg)	Q2D × 3	MiaPaCa pancreatic	300	0	12	0.4	*
Melphalan (3 mg/kg)	Q2D × 3	MCF-7 breast[a]	310	0	19	0.4	*
Melphalan (3 mg/kg)	Q1D × 5	Panc-1 pancreatic	125	0	11	0.3	

Note: Mice were implanted s.c. with 10^7 tumor cells. When the tumor volume reached the volume indicated, the mice were randomized into groups of eight and i.p. drug treatment started at the doses shown.
[a]Female mice implanted with 17-β-estradiol 60-day slow release pellets.
*$P < 0.05$, compared with non-drug-treated control tumor growth rate.

Table 5. Schedule and route dependency of PX-478 antitumor activity

Tumor	Initial tumor volume (mm^3)	PX-478 (mg/kg/day)	Route	Schedule	Regression (%)	Growth delay (days)	Log_{10} cell kill	*P*
MCF-7 breast cancer[a]	190	200	i.p.	Q1D	45	27	1.4	*
	190	120	i.p.	Q1D	50	17	0.9	*
	190	80	i.p.	Q1D × 5	50	44	2.3	*
	310	120	i.p.	Q1D × 5	17	51	2.9	*
	190	120	i.p.	Q2D × 5	79	48	2.5	*
	190	80	i.p.	Q2D × 5	45	37	2.0	*
	310	80	i.p.	Q1D × 5 every 4W × 3	0	60	3.3	*
	310	80	i.p.	Q2D × 5 every 4W × 3	27	62	3.4	*
	310	120	i.p.	QW × 10	0	60	3.3	*
	310	60	i.p.	Q1/2W × 20	0	45	2.5	*
PC-3 prostate cancer	550	100	i.p.	Q1D × 5	72	26	1.3	*
	550	80	i.p.	Q1D × 5	0	13	1.1	*
	550	80	i.v.	Q1D × 5	0	13	1.1	*
	550	25	p.o.	Q1D × 5	0	16	1.3	*

Note: Mice were implanted s.c. with 10^7 tumor cells. When the tumor volume reached a predetermined size, the mice were randomized into groups of eight and drug treatment started at the doses and by the schedules shown.
[a]Female mice implanted with 17-β-estradiol 60-day slow release pellets.
*$P < 0.05$, compared with non-drug-treated control tumor growth rate.

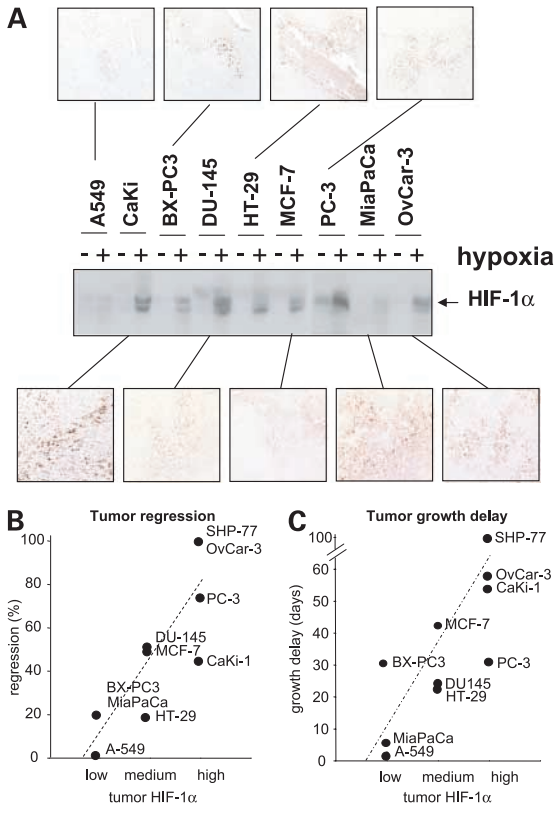

Figure 6. Relationship between PX-478's antitumor activity and tumor HIF-1α. **A,** Western blot (*middle panel*) showing HIF-1α levels in human cancer cell lines grown in air (-) and exposed to hypoxia (1% oxygen) for 16 h (+). Loading was normalized using lamin A (data not shown). Immunohistochemistry staining (*upper and lower panels*) of HIF-1α in tumor xenografts between 150 and 300 mm^3 grown from the same cell lines in *scid* mice. **B,** tumor regression caused by PX-478 in the different tumors with low, medium, and high HIF-1α staining. **C,** tumor growth delay caused by PX-478 in the different tumors with low, medium, and high HIF-1α staining. *Dashed line,* the calculated regression ($P = 0.016$).

HIF-2α is not regulated by hypoxia and does not stimulate the transcription of typical HIF-1 target genes (53). Thus, HIF-2α may have different functions to HIF-1α unrelated to the hypoxia response (54) and, as we now show, is not inhibited by PX-478.

PX-478 showed antitumor activity against a variety of human tumor xenografts characterized by marked tumor regressions and prolonged tumor growth delays. The tumors used are among the most resistant to experimental therapy (70) and were well established (0.1–0.8 cm^3) at the start of treatment. A 5-day course of PX-478 treatment gave log_{10} tumor cell kills up to 3.0. With SHP-77 small cell lung cancer, PX-478 was curative with no histologically detectable tumor at the site of implantation at the end of the study. Antitumor activity was also seen with a single i.p. dose of PX-478 as well as with i.v. and p.o. dose of PX-478. Tumor regression occurred typically 3–10 days after a course of PX-478 treatment and was characterized by extensive apoptosis. Tumor HIF-1α and VEGF were not significantly decreased at this time, although there was a decrease in Glut-1. The ability of PX-478 to cause regressions of very large tumor xenografts is important. The paradigm established from many years of experimental chemotherapy is that larger tumors show a decreased response to drugs and radiation compared with smaller tumors either because of slower growth rates or because of decreased drug access in larger tumors (71–74). PX-478 appears to cause a greater response in larger tumors than in smaller tumors.

The peak PX-478 plasma concentration following a single therapeutic dose of PX-478 was 1500 μM, which is considerably higher than the 5–25 μM required to inhibit HIF-1α in cancer cell lines (55). The plasma half-life of PX-478 was 50 min and the inhibition of tumor HIF-1α,

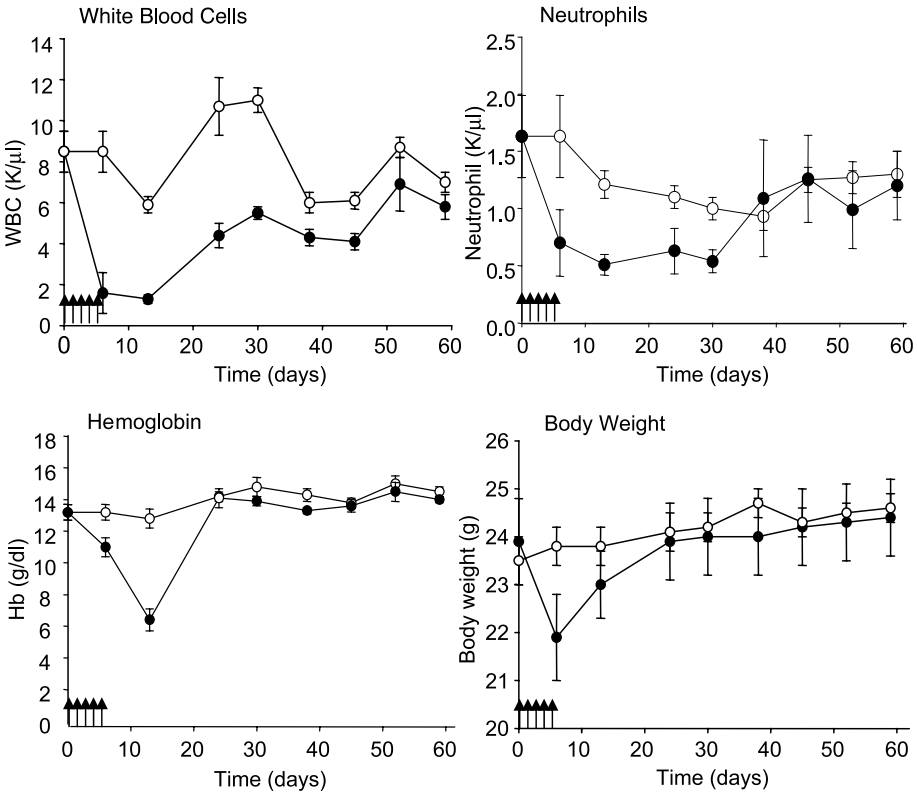

Figure 7. Long-term toxicity of PX-478 by daily i.p. administration for 5 days. Groups of four male C57BL/6 mice received vehicle alone (○) or PX-478 i.p. at a dose of 100 mg/kg (●) dissolved in 0.9% NaCl daily for 5 days. *Arrows,* daily dosing. Blood was collected by retro-orbital puncture into EDTA at the times shown. *Points,* means of four mice; *bars,* SE.

which lasted about 8 h, corresponded to the time that PX-478 in plasma was maintained at above 10 μM. There was a rapid and short-lived decrease in mouse VEGF in plasma. The inhibition of plasma VEGF was more rapid than the inhibition of HIF-1α itself and so is unlikely to be mediated through an effect of PX-478 on VEGF transcription. Platelets and neutrophils are a major source of circulating VEGF (75), which is released by a non-hypoxia-dependent mechanism (76). The turnover of VEGF in plasma occurs with a half-life for human VEGF of around 30 min (77). Thus, the effect of PX-478 on plasma VEGF may be through an inhibition of release by VEGF from blood elements.

The inhibition of tumor growth by PX-478 appears to involve the suppression of tumor HIF-1α. This is

Table 6. Toxicity of PX-478 by daily i.p. administration for 5 days

Parameter	Units	Control	PX-478 (100 mg/kg × 5 days)
Blood cells			
White blood cells	K/μl	4.35 ± 0.52	0.18 ± 0.38*
Neutrophils	K/μl	2.18 ± 0.39	0.13 ± 0.10*
Lymphocytes	K/μl	2.15 ± 0.28	0.29 ± 0.13*
Monocytes	K/μl	0.05 ± 0.01	0.02 ± 0.01
Red blood cells	M/μl	10.7 ± 0.2	9.9 ± 0.3
Hemoglobin	g/dl	14.3 ± 0.1	13.7 ± 0.6
Platelets	K/μl	1112 ± 35	1059 ± 92
Chemistry			
Alkaline phosphatase	U/l	172.6 ± 13.0	222.5 ± 51.5
Glucose	mg/dl	183.7 ± 4.7	115.4 ± 23.3
Alanine aminotransferase	U/l	26.9 ± 5.4	39.9 ± 14.0
Protein	g/dl	5.3 ± 0.1	5.7 ± 0.2
Blood urea nitrogen	mg/dl	10.9 ± 0.7	8.8 ± 1.0
Creatinine	mg/dl	0.2 ± 0.0	0.1 ± 0.0

Note: Groups of four male C57BL/6 mice received PX-478 at a dose of 100 mg/kg/day i.p. for 5 days dissolved in 0.9% NaCl. The mice were killed 24 h after the last dose and blood was taken for chemistry.
*$P < 0.01$, compared with nontreated control value.

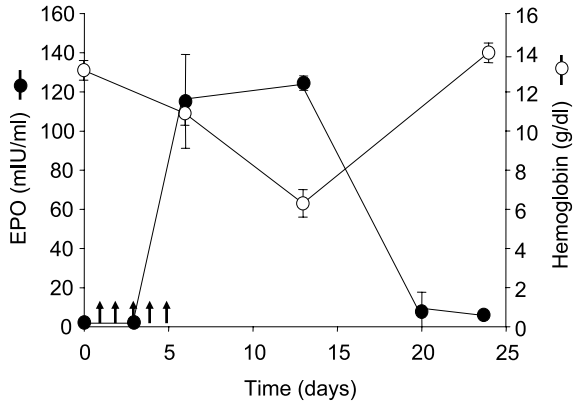

Figure 8. Long-term effects of PX-478 on hemoglobin and plasma erythropoietin levels. Male C57BL/6 mice were treated with PX-478 i.p. at a dose of 100 mg/kg/day for 5 days and blood hemoglobin (○) and plasma erythropoietin (●) levels. Blood was collected into EDTA at the times shown. *Points,* means of four mice; *bars,* SE.

demonstrated by the association between PX-478's antitumor activity and HIF-1α levels in a variety of different human tumor xenografts in *scid* mice. A-549 non-small cell lung cancer, which showed very little HIF-1α staining in xenografts, was resistant to treatment with PX-478. This was the only tumor that did not respond at all to PX-478. Tumor xenografts showing high levels of HIF-1α staining, OvCar-3 ovarian, PC-3 prostate, Caki-1 renal, and SHP-77 small cell lung cancer, all showed marked tumor regression and growth delay caused by treatment with PX-478. The sensitivity of large tumors to PX-478 may relate to the increased HIF-1α staining seen in larger tumors.

The decrease in tumor growth following suppression of tumor HIF-1α could occur through several mechanisms. Much attention has focused on the HIF-1α-dependent production of angiogenic factors such as VEGF in the stimulation of tumor and tumor growth (36, 38, 78). However, some evidence suggests that the major effect of HIF-1α in stimulating tumor growth may not be through increased angiogenesis. Tumors formed by HIF-1α-deficient hepatoma cells show a decreased growth rate compared with tumors from wild-type cells although they have similar vascular parameters (7). Tumors formed from wild-type and HIF-1α −/− knockout mouse embryonic fibroblasts show similar vascular density despite differences in VEGF expression (37). Human pancreatic cancer cells transfected with a dominant-negative HIF-1α form tumors that grow more slowly than nontransfected cells with decreased Glut-1 expression and glucose uptake but no change in angiogenesis measured by microvessel density (6). Based on these results, it has been suggested that compromised glucose uptake and metabolic adaptation following inhibition of HIF-1α, rather than inhibition of angiogenesis, is responsible for the reduced tumorigenicity (6, 7, 37). This is consistent with what we found with PX-478, which gave a relatively small decrease in tumor VEGF and no change in tumor vascular parameters, while there was a marked and prolonged decrease in tumor Glut-1.

The major toxicity of PX-478 with a 5-day course of administration to mice was neutropenia. The neutropenia could be an effect of PX-478 on white blood cell formation due to inhibition of VEGF formation (66). The inhibition of erythropoietin formation and red blood cell synthesis consequent to inhibition of HIF-1α (20) was a potential toxic effect of concern. However, plasma erythropoietin levels were not acutely decreased by PX-478 and only decreased later when red blood cell levels were decreased. Thus, it appears that the decrease in erythropoietin is a consequence of decreased red blood cells rather than the cause.

In summary, we have shown that PX-478 has marked antitumor activity including cures against several established human tumor xenografts that is related to the levels of HIF-1α in the tumors. PX-478 is able to cause regressions of even very large tumor xenografts and was curative in one tumor type. The antitumor studies were conducted in conjunction with pharmacokinetic and pharmacodynamic studies showing that PX-478 inhibits tumor HIF-1α and the expression the downstream genes for VEGF and Glut-1. The inhibition of tumor growth appears to correlate with inhibition of glucose metabolism rather than inhibition of angiogenesis.

Acknowledgments

We thank Bethany Skovan, Alan Toppin, and Nancy Hoogerwerf for help with the antitumor studies and the Arizona Cancer Center Biometry Shared Service for help with the statistical analysis of the data.

References

1. Hoeckel M, Schlenger K, Aral B, Mitza M, Schaffer U, Vaupel P. Association between tumor hypoxia and malignant progression in advanced cancer of the uterine cervix. Cancer Res, 1996;56:4509–15.

2. Moulder J, Rockwell S. Tumor hypoxia: its impact on cancer therapy. Cancer Metastasis Rev, 1987;5:313–41.

3. Nordsmark M, Hoyer M, Keller J, Nielson OS, Jensen OM, Overgaard J. The relationship between tumor oxygenation and cell proliferation in human soft tissue sarcomas. Int J Radiat Oncol Biol Phys, 1996;35:701–8.

4. Sartorelli AC. Therapeutic attack of hypoxic cells of solid tumors. Cancer Res, 1988;48:775–8.

5. Goonewardene TI, Sowter HM, Harris, AL. Hypoxia-induced pathways in breast cancer. Microsc Res Tech, 2002;59:41–8.

6. Chen J, Zhao S, Nakada K, et al. Dominant-negative hypoxia-inducible factor-1α reduces tumorigenicity of pancreatic cancer cells through the suppression of glucose metabolism. Am J Pathol, 2003;162:1283–91.

7. Williams KJ, Telfer L, Airley RE, et al. A protective role for HIF-1 in response to redox manipulation and glucose deprivation: implications for tumorigenesis. Oncogene, 2002;21:282–90.

8. Brizel DM, Scully SP, Harrelson JM, et al. Tumor oxygenation predicts for the likelihood of distant metastases in human soft tissue sarcoma. Cancer Res, 1996;56:941–3.

9. Hanahan D, Folkman J. Patterns and emerging mechanisms of the angiogenic switch during tumorigenesis. Cell, 1996;86:353–64.

10. Ishibashi H, Nakagawa K, Nakashima Y, Sueishi K. Conditioned media of carcinoma cells cultured in hypoxic microenvironment stimulate angiogenesis *in vitro*; relationship to basic fibroblast growth factor. Virchows Arch, 1995;425:561–8.

11. Wang GL, Jiang BH, Rue EA. Hypoxia-inducible factor I is a basic-helix-loop-helix-PAS heterodimer regulated by cellular O_2 tension. Proc Natl Acad Sci USA, 1995;92:5510–4.

12. Dachs GU, Tozer GM. Hypoxia modulated gene expression: angiogenesis, metastasis and therapeutic exploitation. Eur J Cancer, 2000; 36:1649–60.

13. Semenza GL. HIF-1: mediator of physiological and pathophysiological responses to hypoxia. J Am Phys Soc, 2000;88:1474–80.

14. Semenza GL. Hypoxia, clonal selection, and the role of HIF-1 in tumor progression. Crit Rev Biochem Mol Biol, 2000;35:71–103.

15. Beasley N, Leek R, Alam M, et al. Hypoxia-inducible factors HIF-1α and HIF-2α in head and neck cancer: relationship to tumor biology and treatment outcome in surgically resected patients. Cancer Res, 2002; 62:2493–7.

16. Chilov D, Camneish G, Kvietikova I, Ziegler U, Gassmann M, Wenger RH. Induction and nuclear translocation of hypoxia-inducible factor-1 (HIF-1): heterodimerization with ARNT is not necessary for nuclear accumulation of HIF-1α. J Cell Sci, 1999;112:1203–12.

17. Minchenko A, Salceda S, Bauer T. Hypoxia regulatory elements of the human vascular endothelial growth factor gene. Cell Mol Biol Res, 1994; 40:35–9.

18. Kallio PJ, Wilson WJ, O'Brien S, Makino Y, Poellinger L. Regulation of the hypoxia-inducible factor-1a by the ubiquitin-proteasome pathway. J Biol Chem, 1999;274:6519–25.

19. Semenza GL, Roth PH, Frang H, Wang GL. Transcriptional regulation of genes encoding glycolytic enzymes by hypoxia-inducible factor 1. J Biol Chem, 1994;269:23757–63.

20. Wang GL, Semenza GL. Molecular basis of hypoxia-induced erythropoietin expression. Curr Opin Hematol, 1996;3:156–62.

21. Unruh A, Ressel A, Mohamed HG, et al. The hypoxia-inducible factor-1α is a negative factor for tumor therapy. Oncogene, 2003;22: 3213–20.

22. Akakura N, Kobayashi M, Horiuchi I, et al. Constitutive expression of hypoxia-inducible factor-1a renders pancreatic cancer cells resistant to apoptosis induced by hypoxia and nutrient deprivation. Cancer Res, 2001; 61:6548–54.

23. Jung F, Palmer LA, Zhou N, Johns R. Hypoxic regulation of inducible nitric oxide synthase via hypoxia inducible factor-1 in cardiac myocytes. Circ Res, 2000;86:319–25.

24. Maxwell PH, Dachs GU, Gleadle JM, et al. Hypoxia-inducible factor-1 modulates gene expression in solid tumors and influences both angiogenesis and tumor growth. Proc Natl Acad Sci USA, 1997;94:8104–9.

25. Yamashita H, Avraham S, Jiang S, et al. Characterization of human and murine PMP20 peroxisomal proteins that exhibit antioxidant activity *in vitro.* J Biol Chem, 1999;274:29897–904.

26. Pollok BA, Heim R. Using GFP in FRET-based applications. Trends Cell Biol, 1999;9:57–60.

27. Salceda S, Caro J. Hypoxia-inducible factor 1α (HIF-1α) protein is rapidly degraded by the ubiquitin-proteasome system under normoxic conditions: its stabilization by hypoxia depends upon redox-induced changes. J Biol Chem, 1997;272:22642–7.

28. Bruick R, McKnight S. A conserved family of prolyl-4-hydroxylases that modify HIF. Science, 2001;294:1337–40.

29. Bates S, Vousden K. Mechanisms of p53-mediated apoptosis. Cell Mol Life Sci, 1999;55:28–37.

30. Ivan M, Kondo K, Yang H, et al. HIF-1α targeted for VHL-mediated destruction by proline hydroxylation: implications for O_2 sensing. Science, 2001;292:464–8.

31. Huang LE, Arany Z, Livingston DM. Activation of hypoxia inducible transcription factor depends primarily upon redox-sensitive stabilization of its α subunit. J Biol Chem, 1996;271:32253–9.

32. Mahon PC, Hirota K, Semenza GL. FIH-1: a novel protein that interacts with HIF-1a and VHL to mediate repression of HIF-1 transcriptional activity. Genes Dev, 2001;15:2675–86.

33. Ravi R, Mookerjee B, Bhujwalla Z, et al. Regulation of tumor angiogenesis by p53-induced degradation of hypoxia-inducible factor 1 α. Genes Dev, 2000;14:34–44.

34. Chen D, Li M, Luo J, Gu W. Direct interactions between HIF-1 α and Mdm2 modulates p53 function. J Biol Chem, 2003;278:13595–8.

35. Jiang BH, Agani F, Passaniti A, Semenza GL. V-SRC induces expression of hypoxia-inducible factor 1 (HIF-1) and transcription of genes encoding vascular endothelial growth factor and enolase 1: involvement of HIF-1 in tumor progression. Cancer Res, 1997;57:5328–35.

36. Ryan HE, Lo J, Johnson RS. HIF-1 α is required for solid tumor formation and embryonic vascularization. EMBO J, 1998;17:3005–15.

37. Ryan HE, Poloni M, McNulty W, et al. Hypoxia-inducible factor-1α is a positive factor in solid tumor growth. Cancer Res, 2000;60: 4010–5.

38. Carmeliet P, Dor Y, Herbert JM, et al. Role of HIF-1α in hypoxia-mediated apoptosis, cell proliferation and tumor angiogenesis. Nature, 1998;394:485–90.

39. Krieg M, Haas R, Brauch H, Acker T, Flamme I, Plate K. Up-regulation of hypoxia-inducible factors HIF-1a and HIF-2a under normoxic conditions in renal carcinoma cells by von Hippel-Lindau tumor suppressor gene loss of function. Oncogene, 2000;19:5435–43.

40. Maxwell P, Wiesener M, Chang G-W, et al. The tumor suppressor protein VHL targets hypoxia-inducible factors for oxygen-dependent proteolysis. Nature, 1999;399:271–5.

41. Schoenfeld A, Paris T, Eisenberger A, et al. The von Hippel-Lindau tumor suppressor gene protects cells from UV-mediated apoptosis. Oncogene, 2000;19:5851–7.

42. Giatromanolaki A, Koukourakis M, Sivridis E, Turley H, Talks K. Relation of hypoxia inducible factor 1 α and 2 α in operable non-small cell lung cancer to angiogenic molecular profile of tumors and survival. Br J Cancer, 2001;85:881–90.

43. Zagzag D, Zhong H, Scalzetti J, Laughner E, Sitmons J, Semenza G. Expression of hypoxia-inducible factor-1 α in brain tumors: association with angiogenesis, invasion and progression. Cancer, 2000;88:2606–18.

44. Birner P, Schindl M, Obermair A, Plank C, Breitenecker G, Oberhuber G. Over-expression of hypoxia-inducible factor-1α is a marker for an unfavorable prognosis in early-stage invasive cervical cancer. Cancer Res, 2000;60:4693–6.

45. Talks KL, Turley H, Gatter KC, et al. The expression and distribution of the hypoxia-inducible factors HIF-1 α and HIF-2 α in normal human tissues, cancers, and tumor-associated macrophages. Am J Pathol, 2000; 157:411–21.

46. Aebersold DM, Burri P, Beer KT, et al. Expression of hypoxia-inducible factor-1α: a novel predictive and prognostic parameter in the radiotherapy of oropharyngeal cancer. Cancer Res, 2001;61:2911–6.

47. Birner P, Gatterbauer B, Oberhuber H, et al. Expression of hypoxia-inducible factor-1 α in oligodendrogliomas: its impact on prognosis and on neoangiogenesis. Cancer, 2001;92:165–71.

48. Birner P, Schindl M, Obermair A, Breitenecker G, Oberhuber G. Expression of hypoxia-inducible factor-1 α in epithelial ovarian tumors: its impact on prognosis and on response to chemotherapy. Clin Cancer Res, 2001;7:1661–8.

49. Schindl M, Schoppmann SF, Samonigg H, et al. Overexpression of hypoxia-inducible factor 1α is associated with an unfavorable prognosis in lymph node-positive breast cancer. Clin Cancer Res, 2002;8:1831–7.

50. Kaelin W Jr. Molecular basis of the VHL hereditary cancer syndrome. Nat Rev Cancer, 2002;2:673–82.

51. Wiesner M, Munchenhagen P, Berger I, et al. Constitutive activation of hypoxia-inducible genes related to overexpression of hypoxia-inducible factor-1α in clear cell renal carcinomas. Cancer Res, 2001;61:5215–22.

52. Turner KJ, Moore JW, Jones A, et al. Expression of hypoxia-inducible factors in human renal cancer: relationship to angiogenesis and to the von Hippel-Lindau gene mutation. Cancer Res, 2002;62:2957–61.

53. Park S, Dadak AM, Haase VH, Fontana L, Giaccia AJ, Johnson RS. Hypoxia-induced gene expression occurs solely through the action of hypoxia-inducible factor 1α (HIF-1α): role of cytoplasmic trapping of HIF-2α. Mol Cell Biol, 2003;23:4959–71.

54. Brusselmans K, Bono F, Maxwell Y, et al. Hypoxia-inducible factor-2α (HIF-2α) is involved in the apoptotic response to hypoglycemia but not to hypoxia. J Biol Chem, 2001;276:39192–6.

55. Welsh SJ, Williams RR, Kirpatrick DL, Powis G. PX-478, a potent inhibitor of hypoxia-inducible factor-1 (HIF-1) and antitumor agent. Eur J Cancer, 2002;38 Suppl:S90.

56. Kristensen CA, Kristjansen PE, Brunner N, Clarke R, Spang-Thomsen M, Quistorff B. Effect of estrogen withdrawal on energy-rich phosphates and prediction of estrogen dependence monitored by *in vivo* 31P magnetic resonance spectroscopy of four human breast cancer xenografts. Cancer Res, 1995;55:1664–9.

57. Paine GD, Taylor CW, Curtis RA, et al. Human tumor models in the severe combined immune deficient *scid* mouse. Cancer Chemother Pharmacol, 1997;40:209–14.

58. Teicher B. *In vivo* tumor response end points. In: Teicher B, editor. Tumor models in cancer research. Totowa, NJ: Humana Press Inc.; 2002. p. 593–616.

59. Snedecor GW, Cochran WG. The comparison of two samples. Statistical methods. 6th ed. Ames, IA: Iowa State University; 1967. p. 91–119.

60. Weidner N, Semple J, Welch W, Folkman J. Tumor angiogenesis and metastasis: correlation in invasive breast carcinoma. N Engl J Med, 1991;324:1–8.

61. Welsh SJ, Williams RR, Birmingham A, Newman DJ, Kirkpatrick DL, Powis G. The thioredoxin redox inhibitors 1-methylpropyl 2-imidazolyl disulfide and pleurotin inhibit hypoxia-induced factor 1a and vascular endothelial growth factor formation. Mol Cancer Ther, 2003; 2:235–43.

62. Gleadle JM, Ratcliffe PJ. Induction of hypoxia-inducible factor-1, erythropoietin, vascular endothelial growth factor, and glucose transporter-1 by hypoxia: evidence against a regulatory role for Src kinase. Blood, 1997;89:503–9.

63. Forsythe JA, Jiang BH, Iyer NV, et al. Activation of vascular endothelial growth factor gene transcription by hypoxia-inducible factor 1. Mol Cell Biol, 1996;16:4604–13.

64. Gown AM, Willingham MC. Improved detection of apoptotic cells in archival paraffin sections: immunohistochemistry using antibodies to cleaved caspase 3. J Histochem Cytochem, 2002;50:449–54.

65. Fang J, Yan L, Shing Y, Moses MA. HIF-1α-mediated up-regulation of vascular endothelial growth factor, independent of basic fibroblast growth factor is important in the switch to the angiogenic phenotype during early tumorigenesis. Cancer Res, 2001;61:5731–5.

66. Bellamy W, Richter L, Sirjani D, et al. Vascular endothelial cell growth factor is an autocrine promoter of abnormal localized immature myeloid precursors and leukemia progenitor formation in myelodysplastic syndromes. Blood, 2000;97:1427–34.

67. Zhang JZ, Behrooz A, Ismail-Beigi F. Regulation of glucose transport by hypoxia. Am J Kidney Dis, 1999;34:1–25.

68. Joost HG, Thorens B. The extended GLUT-family of sugar/polyol transport facilitators: nomenclature, sequence characteristics, and potential function of its novel members. Mol Membr Biol, 2001;18: 247–56.

69. Airley R, Loncaster J, Davidson S, et al. Glucose transporter *glut-1* expression correlates with tumor hypoxia and predicts metastasis-free survival in advanced carcinoma of the cervix. Clin Cancer Res, 2001; 7:928–34.

70. Kerbel RS. Human tumor xenografts as predictive preclinical models for anticancer drug activity in humans. Cancer Biol Ther, 2003;2:108–13.

71. Paulsen JE, Elgjo K. Effect of tumor size on the *in vivo* growth inhibition of human colon carcinoma cells (HT-29) by colon mitosis inhibitor. In Vivo, 2001;15:397–401.

72. Steel GG, Adams K, Stanley J. Size dependence of the response of Lewis lung tumors to BCNU. Cancer Treat Rep, 1976;60:1743–8.

73. Thomas J. A lung colony clonogenic cell assay for human malignant melanoma in immune-suppressed mice and its use to determine chemosensitivity, radiosensitivity and the relationship between tumor size and response to therapy. Br J Surg, 1979;66:696–700.

74. Van Laar JA, Rustum YM, Van der Wilt CL, et al. Tumor size and origin determine the antitumor activity of cisplatin or 5-fluorouracil and its modulation by leucovorin in murine colon carcinomas. Cancer Chemother Pharmacol, 1996;39:79–89.

75. Taichman NS, Young S, Cruchley AT, Taylor P, Paleolog E. Human neutrophils secrete vascular endothelial growth factor. J Leuk Biol, 1997;62:397–400.

76. Koehne P, Willam C, Strauss E, Schindler R, Eckardt KU, Buhrer C. Lack of hypoxic stimulation of VEGF secretion from neutrophils and platelets. Am J Physiol, 2000;279:H817–24.

77. Eppler SM, Combs DL, Henry TD, et al. A target-mediated model to describe the pharmacokinetics and hemodynamic effects of recombinant human vascular endothelial growth factor in humans. Clin Pharmacol Ther, 2002;72:20–32.

78. Buchler P, Reber HA, Buchler M, et al. Hypoxia-inducible factor 1 regulates vascular endothelial growth factor expression in human pancreatic cancer. Pancreas, 2003;26:56–64.